

---

# Learning to Feel the Future: DreamTacVLA for Contact-Rich Manipulation

---

Guo Ye<sup>\*1</sup> Zexi Zhang<sup>\*1</sup> Xu Zhao<sup>1</sup> Shang Wu<sup>1</sup> Haoran Lu<sup>1</sup> Shihan Lu<sup>1</sup> Han Liu<sup>1</sup>

## Abstract

Vision-Language-Action (VLA) models have shown remarkable generalization by mapping web-scale knowledge to robotic control, yet they remain blind to physical contact. Consequently, they struggle with contact-rich manipulation tasks that require reasoning about force, texture, and slip. While some approaches incorporate low-dimensional tactile signals, they fail to capture the high-resolution dynamics essential for such interactions. To address this limitation, we introduce **DreamTacVLA**, a framework that grounds VLA models in contact physics by learning to feel the future. Our model adopts a hierarchical perception scheme in which high-resolution tactile images serve as micro-vision inputs coupled with wrist-camera local vision and third-person macro vision. To reconcile these multi-scale sensory streams, we first train a unified policy with a Hierarchical Spatial Alignment (HSA) loss that aligns tactile tokens with their spatial counterparts in the wrist and third-person views. To further deepen the model’s understanding of fine-grained contact dynamics, we finetune the system with a tactile world model that predicts future tactile signals. To mitigate tactile data scarcity and the wear-prone nature of tactile sensors, we construct a hybrid large-scale dataset sourced from both high-fidelity digital twin and real-world experiments. By anticipating upcoming tactile states, DreamTacVLA acquires a rich model of contact physics and conditions its actions on both real observations and imagined consequences. Across contact-rich manipulation tasks, it outperforms state-of-the-art VLA baselines, achieving up to **95%** success, highlighting the importance of understanding physical contact for robust, touch-aware robotic agents.

## 1 Introduction

Vision-Language-Action (VLA) models enable robots to leverage web-scale knowledge for general-purpose manipulation (Team et al., 2024; Kim et al., 2024; Brohan et al., 2024), but their success is largely limited to visually guided tasks. In contact-rich scenarios such as insertion or deformable object manipulation, VLA agents often fail due to the lack of tactile awareness. Although recent work has introduced tactile inputs into VLA pipelines (Huang et al., 2025; Cheng et al., 2025), these approaches rely on low-dimensional force or torque signals that are sparse and ambiguous, providing little information about how or where contact occurs.

To create robots capable of human-level dexterity, tactile sensing must be high-resolution and integrated across multiple spatial scales. However, scaling such tactile-aware models poses a fundamental data challenge: visual tactile sensors are expensive and fragile, making large-scale real-world data collection prohibitively costly. We therefore construct a large-scale tactile data generation pipeline in simulation, complemented by a high-fidelity digital twin of the tactile sensor and manipulation environment to improve sim-to-real transfer. This hybrid strategy enables scalable tactile learning while maintaining physical realism.

However, data alone are not sufficient. Contact-rich manipulation inherently requires reasoning across multiple spatial scales, from global task context to fine-grained contact events. This motivates our hierarchical perception framework, which organizes sensory inputs into three levels: **macro** for arm-level task context, **local** for end-effector visual guidance, and **micro** for fingertip tactile cues such as slip and insertion forces (Figure 3).

Integrating information across these scales is non-trivial, as tactile signals differ fundamentally from visual inputs in both form and semantics. To bridge this modality gap, we establish spatial correspondence between vision and touch by mapping tactile activations to their locations in wrist and third-person views using robot kinematics and camera calibration. Based on this alignment, we learn a unified latent representation that enables joint reasoning over what the robot sees and what it feels.

However, alignment alone does not guarantee that VLA

---

<sup>1</sup>Department of Computer Science, Northwestern University. Correspondence to: Guo Ye <guoye2018@u.northwestern.edu>.

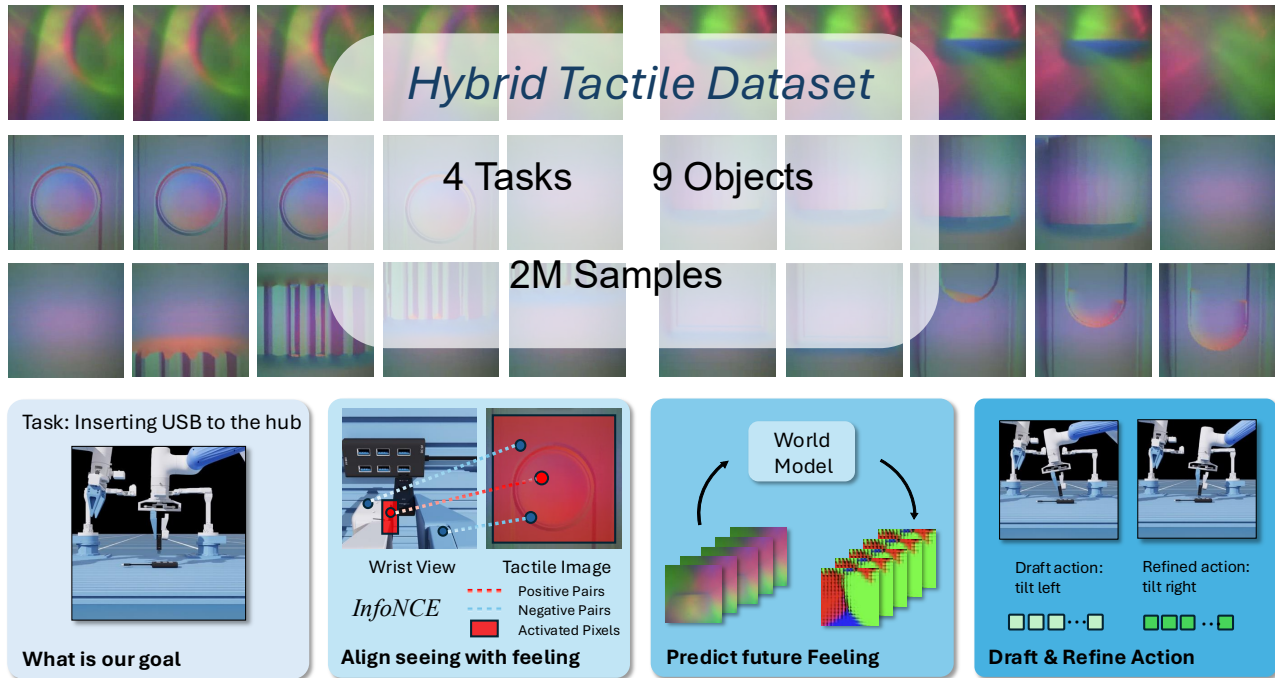


Figure 1. Hybrid tactile dataset and the Tactile-DreamVLA inference mechanism. (Top) We collect a large-scale tactile dataset covering 4 manipulation tasks and 9 objects, totaling 2M tactile frames. (Bottom) Our Think–Dream–Act loop executes each step of the policy in two passes. In the **Think** stage, the policy proposes a draft action using the current state and a null tactile prediction. In the **Dream** stage, a frozen V-JEPA2 world model forecasts the tactile outcome of that draft action. In the **Act** stage, the policy integrates both the real observation and the predicted tactile feedback to refine the action. This enables fine-grained corrections for contact-rich manipulation.

models will meaningfully use tactile information. Since vision–language backbones are pretrained without touch, naively appending tactile inputs often leads the model to ignore them. This is problematic because tactile sensing uniquely captures fine-grained contact physics, such as slip and local deformation, that vision cannot provide.

Meanwhile, conventional world models focus on predicting full RGB observations in high-dimensional latent spaces, which is computationally expensive and often unstable. In contrast, vision-based tactile images exhibit simpler structure and more constrained dynamics while remaining highly informative about contact interactions. Motivated by this, we introduce a tactile-centric world model that predicts future tactile signals in latent space (Figure 1). This predictive objective compels the model to actively use tactile information and learn the evolution of local contact physics.

Nevertheless, traditional world-model pipelines typically rely on a reward function and an MPC-style planner to derive actions, making them computationally heavy and difficult to deploy in contact-rich manipulation. To avoid this complexity, we adopt a two-stage learning framework that enables tactile-driven policies to emerge directly.

In the first stage, we train the policy using only the unified multimodal perception module, encouraging it to produce a draft action from aligned multi-scale observations. In

the second stage, we activate the tactile world model to predict future tactile states, which are fused with the policy to refine actions based on anticipated contact outcomes. This design allows DreamTacVLA to reason over both present observations and imagined tactile futures without explicit planning, remaining lightweight and end-to-end trainable.

**In summary, we make the following contributions:**

- We introduce a novel contrastive loss for spatial alignment on multi-scale sensor data. This method aligns diverse perceptions into a single unified latent space.
- We introduce a tactile world model trained as a self-supervised objective to “dream” the future. By predicting high-resolution tactile signals, this model learns an implicit understanding of contact physics and material interactions.
- We propose a two-stage “Think-Dream-Act” policy that uses this “dreaming” capability for refinement. The policy first thinks of a draft action, then dreams its tactile consequences using the world model, and finally acts by outputting a refined, more precise command.
- We introduce a large-scale simulated tactile dataset, paired with a high-fidelity digital twin, which enables dense and diverse tactile supervision that would be prohibitively expensive to obtain in the real world.

## 2 Related Work

### 2.1 Vision-Language-Action (VLA) Models

Vision-Language-Action (VLA) models have become a dominant paradigm for general-purpose robot control, demonstrating strong cross-task and cross-embodiment generalization by scaling data, model capacity, and action representations (Brohan et al., 2022; 2024; Team et al., 2024; Kim et al., 2024; Black et al., 2024). Recent advances also improve VLA effectiveness via modular architectures and stronger adaptation recipes, boosting real-robot performance and efficiency (Li et al., 2024; Kim et al., 2025). Despite these advances, most VLAs remain predominantly vision-centric and continue to struggle in contact-rich manipulation where tactile reasoning is critical, motivating efforts to incorporate touch into generalist policies via post-hoc adaptation (Jones et al., 2025). Detailed discussion and additional references please refer to Appendix F.1.

### 2.2 Multimodal Grounding for Robotics

Multimodal grounding aligns perception with physical interaction by incorporating spatial and tactile cues beyond RGB. Spatially enhanced VLAs introduce explicit or implicit geometric priors (e.g., egocentric 3D encodings, point clouds, or structured traces) to improve geometric reasoning and manipulation robustness (Qu et al., 2025; Li et al., 2025; Lin et al., 2025). Tactile grounding further augments contact awareness, yet many policies still rely on low-dimensional force or compressed touch signals that miss fine-grained contact geometry; recent work instead fuses high-resolution tactile sensing for multimodal reasoning and reactive correction in contact-rich tasks (Liu et al., 2025; Huang et al., 2025; Cheng et al., 2025; Xue et al., 2025). In parallel, tactile representation learning targets transferable visuotactile embeddings via self-supervision or cross-modal alignment (Yang et al., 2024; Fu et al., 2024; Higuera et al., 2024). Our work leverages vision-based tactile micro-vision to capture texture, geometry, and shear-induced slip for fine-grained contact modeling. Detailed discussion and additional references please refer to Appendix F.2 F.3.

### 2.3 Predictive World Models in Robotics

Predictive world models learn latent dynamics that capture temporal and physical regularities, enabling agents to anticipate future evolution for decision making (Ha & Schmidhuber, 2018; Hafner et al., 2023). Large-scale pretraining further yields structured representations whose latent spaces encode semantics and dynamics beneficial for downstream control (Nair et al., 2022; Assran et al., 2025). Recent VLA architectures integrate such predictive modeling into policy learning by conditioning actions on latent rollouts (Zhang et al., 2025; Cen et al., 2025). In the tactile domain, prior work mostly studies representation learning or autoregressive tactile prediction (Heng et al., 2025), whereas our work

predicts high-resolution tactile futures and aligns them with visual observations for fine-grained contact reasoning. Detailed discussion and additional references please refer to Appendix F.4.

## 3 Methodology

Our model, DreamTacVLA, is designed to learn robust, contact-rich manipulation skills by integrating high-resolution vision-based tactile images with standard visual (third-person and wrist camera) and language inputs. Our architecture, shown in Figure 2, is a unified, end-to-end framework built on a shared LLM backbone. It consists of three main components:

**Multimodal Encoders ( $E_\psi$ ):** We employ modality-specific encoders to process all sensory streams: a CLIP ViT encoder for third-person and wrist images, and also for language prompts, and an MLP for robot state. Each modality produces a set of feature tokens that are concatenated into a unified token sequence. During Stage 1, the vision and tactile encoders are trained with our Hierarchical Spatial Alignment (HSA) loss. This yields a spatially-aligned multimodal representation  $H_{align}^{(t)}$ .

**Tactile World Model ( $W_\phi$ ):** A world model that acts as an implicit physics engine. It takes the current tactile image and a draft action  $a_{draft}^{(t)}$  to predict the future sensory state  $H_{dream}^{(t+N)}$ , where  $N$  is the future horizon predicted by the model.

**Unified Policy ( $\pi_\theta$ ):** Our policy consists of a CLIP-based (Radford et al., 2021) multimodal encoder paired with an Action Expert transformer. The Action Expert operates in two passes: first, it drafts an action  $a_{draft}^{(t)}$  based only on the current state. Second, it generates a refined, final action  $a_{final}^{(t)}$  based on both the current state  $H_{align}^{(t)}$  and the dreamed future state  $H_{dream}^{(t+N)}$ .

This Think–Dream–Act loop, implemented through our two-stage training procedure, enables the policy to internally verify its decisions by forecasting the physical consequences of candidate actions prior to execution.

### 3.1 Stage1: Pre-training Spatial Alignment & World Model

The foundational goal of this stage is to train the model’s encoders to understand where the tactile sensor is in relation to the visual world, and to learn a baseline action policy. This is achieved by simultaneously optimizing two losses: the action loss ( $\mathcal{L}_{action}$ ) and our novel Hierarchical Spatial Alignment ( $\mathcal{L}_{HSA}$ ) loss.

#### 3.1.1 HIERARCHICAL SPATIAL ALIGNMENT (HSA)

To enable the model to fuse information across the three visual scales (TPV, wrist, and tactile), it must understand

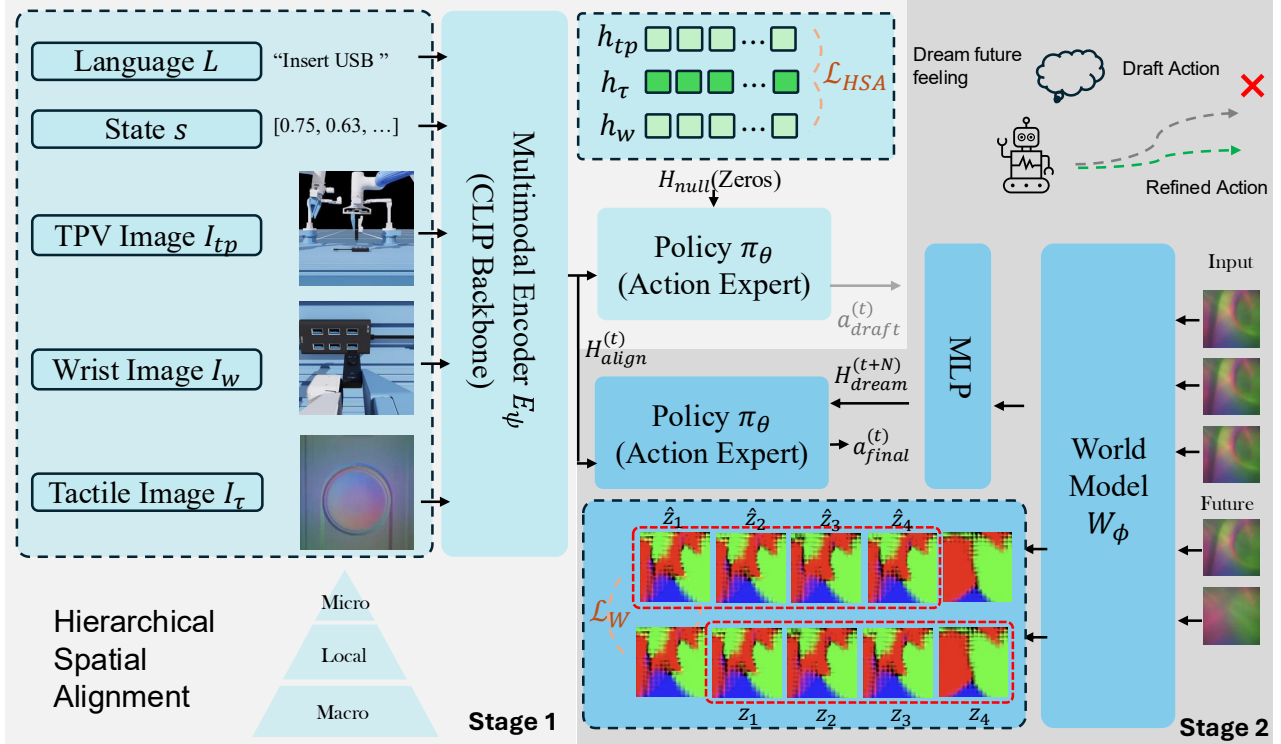


Figure 2. The proposed framework operates in two stages. **Stage 1 (Left)**: A multimodal encoder  $E_\psi$  processes diverse inputs. This stage employs Hierarchical Spatial Alignment (HSA) to effectively fuse the features from different modalities, guided by the  $\mathcal{L}_{HSA}$  and  $\mathcal{L}_W$  losses. A policy  $\pi_\theta$  is trained to output an initial draft action  $a_{draft}^{(t)}$ . **Stage 2 (Right)**: A world model  $W_\phi$  is trained to predict future tactile image sequences. The policy “dreams” the future tactile feeling (e.g.,  $H_{dream}^{(t+N)}$ ) that would result from its draft action. This predicted future is fed into an MLP, allowing the policy to refine its plan and output a more robust final action  $a_{final}^{(t)}$ .

where the tactile sensor is located within the other camera views. We enforce this understanding through a Hierarchical Spatial Alignment (HSA) loss.



Figure 3. The three-scale visual hierarchy of our model. Our framework fuses information from three distinct visual modalities. Our Hierarchical Spatial Alignment (HSA) loss is designed to explicitly ground the micro-vision (what the robot feels) within the local and macro visual contexts (what the robot sees).

First, using the robot’s forward kinematics and calibrated camera parameters (extrinsics  $E_{tp}, E_w$  and intrinsics  $K_{tp}, K_w$ ), we find the 3D pose of the tactile sensor  $P_{sensor}^{(t)} \in SE(3)$ . We then project this pose to find its corresponding 2D bounding box in both camera views:  $\mathcal{B}_w^{(t)}$  in the wrist view and  $\mathcal{B}_{tp}^{(t)}$  in the third-person view.

From an intermediate layer of the LLM, we extract the fea-

ture tokens  $H_{mid}^{(t)}$ . We compute three mean-pooled feature vectors: (1)  $h_\tau$ : The mean-pooled embedding of all tactile tokens  $Z_\tau^{(t)}$ . (2)  $h_w$ : The mean-pooled embedding of all wrist-view tokens whose spatial positions fall within the projected bounding box  $\mathcal{B}_w^{(t)}$ . (3)  $h_{tp}$ : The mean-pooled embedding of all third-person view tokens within  $\mathcal{B}_{tp}^{(t)}$ .

We then apply a token-level InfoNCE contrastive loss to pull these corresponding representations together. The loss for aligning the tactile view with the wrist view is:

$$\mathcal{L}_{HSA-W} = -\log \frac{\exp\left(\frac{h_\tau \cdot h_w}{\kappa}\right)}{\exp\left(\frac{h_\tau \cdot h_w}{\kappa}\right) + \sum_{i=1}^{N_k} \exp\left(\frac{h_\tau \cdot h_{w,i}^{neg}}{\kappa}\right)}. \quad (3.1)$$

where  $h_{w,i}^{neg}$  are  $N_k$  negative samples (e.g., tokens from other regions or other images in the batch) and  $\kappa$  is a temperature parameter. A similar loss,  $\mathcal{L}_{HSA-TP}$ , is computed between  $h_\tau$  and  $h_{tp}$ . The total alignment loss is:

$$\mathcal{L}_{HSA} = \mathcal{L}_{HSA-W} + \mathcal{L}_{HSA-TP}. \quad (3.2)$$

This loss explicitly forces the model to learn that the *micro-*

vision tactile image corresponds to specific, localized regions in the *macro-vision* camera feeds.

### 3.1.2 ACTION LOSS

The Action Expert is trained with a behavior cloning objective. Given the aligned multimodal tokens, it predicts an  $H$ -step action sequence  $\hat{A}^{(t)}$ , which we supervise using the expert actions  $A^{(t)}$ . We apply an  $\ell_1$  loss over the horizon:

$$\mathcal{L}_{\text{action}} = \frac{1}{H} \sum_{j=0}^{H-1} \left\| \hat{a}_j^{(t)} - a_j^{(t)} \right\|_1. \quad (3.3)$$

This trains the action expert to reproduce expert trajectories from the fused multimodal inputs. The total loss for Stage 1 is a weighted sum of these two objectives:

$$\mathcal{L}_{\text{Stage 1}} = \mathcal{L}_{\text{action}} + \lambda_{\text{HSA}} \mathcal{L}_{\text{HSA}}. \quad (3.4)$$

Upon completion of this stage, we have a competent baseline policy that understands where its tactile sensor is and how to perform basic actions.

In this stage, the goal is to train the HSA encoders and a baseline policy. We don't have a trained world model yet, so we cannot generate a dreamed future. To solve this, we feed the policy a zero-tensor in place of the input  $H_{\text{dream}}^{(t+N)}$ .

### 3.1.3 PRETRAINED TACTILE WORLD MODEL ( $W_\phi$ )

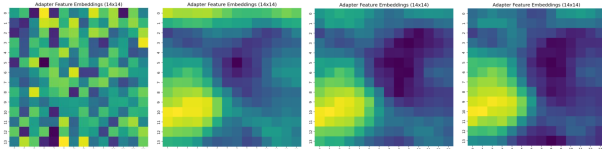


Figure 4. Visualization of the world model's predicted future-state embedding  $H_{\text{dream}}$  across training. Initially, the embedding is noisy and unstructured, indicating weak predictive ability. As training advances, the embedding becomes increasingly concentrated and stable, revealing that the world model is learning a coherent representation of future tactile-visual dynamics.

A key component of our architecture is a pre-trained, frozen world model,  $W_\phi$ , which functions as a powerful tactile feature extractor. We pre-train this model on a large, unlabeled dataset of tactile image sequences.  $W_\phi$  (V-JEPA2 (Assran et al., 2025)) is trained to be an expert in tactile physics. Its job is to take a tactile image  $I_\tau$  and encode it in a rich, latent embedding  $z_\tau$  that captures the underlying physical state, as shown in Figure 4.

$$z_\tau = W_\phi(I_\tau). \quad (3.5)$$

Throughout all subsequent training stages,  $W_\phi$  remains frozen, providing a stable and high-quality embedding of tactile information.

## 3.2 Stage 2: Finetuning with a Latent Dream

The goal of this stage is to finetune the entire pre-trained system ( $\pi_\theta$  and  $E_\psi$ ) to learn a robust model of physical interaction. We achieve this by introducing a lightweight Forecasting MLP ( $F_\eta$ ), which learns to dream of the latent sensory consequences of a draft action. This predicted future tactile embedding is then fed back to the policy, allowing it to make a more informed, physically-grounded final decision. During this stage, the main encoders ( $E_\psi$ ) and the policy ( $\pi_\theta$ ) are finetuned, while the new forecasting MLP ( $F_\eta$ ) is trained from scratch. The pre-trained tactile world model ( $W_\phi$ ) remains frozen to act as a stable feature extractor. We continue to apply the action loss ( $\mathcal{L}_{\text{action}}$ ) and the Hierarchical Spatial Alignment loss ( $\mathcal{L}_{\text{HSA}}$ ), while adding the new latent forecasting loss,  $\mathcal{L}_W$ . The Think-Dream-Act pipeline in this stage now functions as follows:

**THINK:** Policy  $\pi_\theta$  generates a draft action  $a_{\text{draft}}^{(t)}$  based on the current aligned state  $H_{\text{align}}^{(t)}$  and the null dream  $H_{\text{null}}$ .

**DREAM:** MLP Forecasting  $F_\phi$  predicts the future latent tactile state,  $H_{\text{dream}}^{(t+N)}$ . It takes two inputs: the current tactile embedding (from the frozen  $W_\phi$ ) and the draft action (from the policy):

$$H_{\text{dream}}^{(t+N)} = F_\eta(z_\tau^{(t)}, a_{\text{draft}}^{(t)}). \quad (3.6)$$

**ACT:** This predicted future embedding,  $H_{\text{dream}}^{(t+N)}$ , is fed back to the policy  $\pi_\theta$  along with the current state  $H_{\text{align}}^{(t)}$  to produce the refined, final action  $a_{\text{final}}^{(t)}$ .

## 4 Experiments

The primary hypothesis of this work is that for a robotic agent to achieve robust, contact-rich manipulation, it must not only react to the physical world but reason about its physical consequences. We posit that this capability is unlocked by combining two key components: (1) a high-resolution, spatially-grounded understanding of the current contact state (enabled by HSA) and (2) a predictive world model that can dream the future tactile images. We design our experiments to rigorously validate this hypothesis by dissecting our model's contributions.

### 4.1 Experimental Setup

#### 4.1.1 IMPLEMENTATION DETAILS

The full system consists of a language-conditioned policy, modality-specific encoders, a frozen tactile world model with lightweight adapters, and an action transformer expert. Below we detail each component.

**Model Architecture.** Policy and Encoders: The policy  $\pi_\theta$  (Language Backbone) is initialized from a pretrained CLIP (clip-vit-large-patch14) model (Radford et al., 2021)

Table 1. Task Success Rates (%) in Real-world (100 trials). Results are reported as mean  $\pm$  standard deviation over 3 runs.

| Model                               | Peg-in-Hole                       | USB Insert                        | Gear Assembly                     | Pen Stabilize                     |
|-------------------------------------|-----------------------------------|-----------------------------------|-----------------------------------|-----------------------------------|
| ACT (Zhao et al., 2023)             | 35.2 $\pm$ 0.7%                   | 62.6 $\pm$ 0.5%                   | 22.4 $\pm$ 0.8%                   | 19.3 $\pm$ 0.6%                   |
| Diffusion Policy (Chi et al., 2025) | 35.5 $\pm$ 0.9%                   | 56.3 $\pm$ 0.8%                   | 33.1 $\pm$ 0.7%                   | 30.4 $\pm$ 0.9%                   |
| $\pi$ 0 (Black et al., 2024)        | 48.7 $\pm$ 1.0%                   | 59.4 $\pm$ 0.9%                   | 45.2 $\pm$ 1.1%                   | 41.0 $\pm$ 0.8%                   |
| ACT (w/ Tactile)                    | 45.6 $\pm$ 0.3%                   | 63.1 $\pm$ 0.4%                   | 40.2 $\pm$ 0.2%                   | 39.1 $\pm$ 0.7%                   |
| Ours (HSA-Only, No Dream)           | 60.8 $\pm$ 0.9%                   | 63.7 $\pm$ 0.8%                   | 51.5 $\pm$ 1.0%                   | 42.9 $\pm$ 0.7%                   |
| Ours (No HSA, Dream-Only)           | 75.4 $\pm$ 0.8%                   | 75.2 $\pm$ 0.7%                   | 64.9 $\pm$ 0.6%                   | 68.5 $\pm$ 0.9%                   |
| <b>Ours (HSA &amp; Dream)</b>       | <b>95.0 <math>\pm</math> 0.2%</b> | <b>85.7 <math>\pm</math> 0.6%</b> | <b>81.1 <math>\pm</math> 0.4%</b> | <b>74.6 <math>\pm</math> 0.5%</b> |

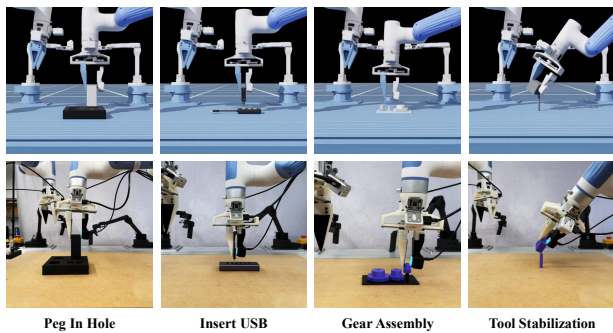


Figure 5. Task suite used to evaluate DreamTacVLA. From left to right: Peg-in-Hole, USB Insert, Gear Assembly, and Tool Stabilization. Each task demands precise, contact-rich manipulation, including aligning tight tolerances, detecting slip, or maintaining stable tool contact. It provides a comprehensive benchmark for assessing tactile-aware policies.

and finetuned on our dataset. This CLIP model is also responsible for aligning wrist camera and tactile images. The tactile image ( $I_\tau$ ) encoder is a V-JEPA2 model (Assran et al., 2025) (ViTL/ViTG), initialized from its official pre-trained weights.

**Action Expert:** Our action expert is an action transformer, which is trained to predict a 7-DOF action (6D end-effector pose + 1D gripper state) over a 45-step horizon. The same horizon is used during inference.

**World Model and Tactile Adaptation.** We employ V-JEPA2 ViT-L/Vit-G as our tactile world model, pretrained on tactile images from our dataset and frozen during policy training. The pretrained encoder (in the case of ViT-L) produces 1024-dimensional patch embeddings. To enable the policy to refine its draft actions using tactile context while still preserving the pretrained representation, we insert a lightweight residual adapter after the frozen encoder. The adapter processes all patch tokens (not just the CLS token) through a 3-layer bottleneck MLP with GELU activations and dropout ( $p=0.1$ ). A learnable residual scale, initialized to 0.1, controls the magnitude of adapter features added to the frozen representations. We aggregate

the adapted patches using learned attention pooling, where a single learnable query token attends to all 196 adapted patches via 8-head multi-head attention. This architecture adds only 5.5M trainable parameters (1.8% overhead) to the 300M frozen ViT-L, enabling efficient task-specific adaptation while retaining the world model’s learned dynamics. The adapter and pooling weights are optimized jointly with the policy using AdamW (lr= $1e-5$ , weight decay= $1e-4$ ).

#### 4.1.2 SIMULATION & HARDWARE

We conduct experiments in both simulation and the real world. Our simulation environment is built in IsaacSim (NVIDIA). To enable realistic, high-fidelity tactile data collection, we integrate a physics-based tactile sensor model based on the work of TacEx (Nguyen et al., 2024). This integration follows the Taxim (Si & Yuan, 2022) style optical and texture-based tactile simulation approach, which synthesizes gel deformation appearance through light-transport modeling and marker-texture warping. This allows us to generate realistic, high-resolution tactile images that closely mimic our real-world sensors, which is critical for large-scale data collection (1000 demonstrations per task) with randomized object poses in parallel environments. Our real-world setup uses a Dobot Xtrainer platform with a parallel gripper, two high-resolution GelSight (Yuan et al., 2017) sensors, and two Realsense D405 cameras as wrist and third-person cameras. We collect 100 expert demonstrations for each real-world task. Figure 7 provides a qualitative comparison of the data streams from simulation and real-world hardware execution.

**Tasks.** We evaluate four challenging contact-rich tasks. As shown in Figure 5. 1) Peg-in-Hole: A classic robotics task requiring high precision. The port is partially occluded, forcing the policy to rely on tactile feedback for the final alignment. 2) USB Insertion: Inserting a USB-A plug into a port. This task has extremely tight tolerances (sub-millimeters) that are ambiguous from vision alone. 3) Gear Assembly: Sliding a small gear onto a shaft. This requires aligning the gear’s hole with the shaft, a task that easily failed due

to misalignment. 4) Tool Stabilization: The agent grips a cube and uses one of its vertices to support a thin vertical cylinder on the tabletop, maintaining the cylinder in a stable upright pose under small disturbances. We constructed a hybrid dataset consists of approximately 80% simulated demonstrations and 20% real-world demonstrations across four task categories, as illustrated in Figure 6.

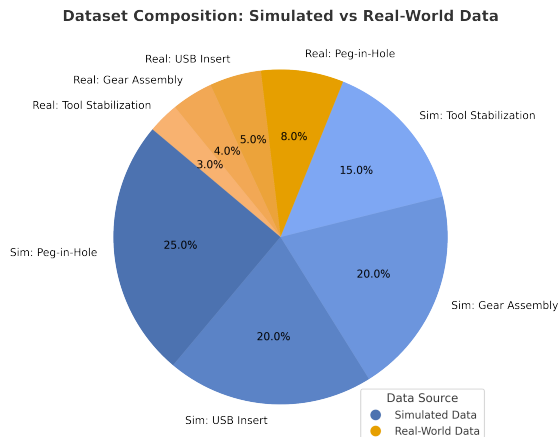


Figure 6. The dataset consists of 80% simulated demonstrations and 20% real-world demonstrations, each containing four task categories: Peg-in-Hole, USB Insert, Gear Assembly, and Tool Stabilization. Blue segments represent simulated data, while orange segments denote real-world data.

**Baselines.** We compare DreamTacVLA against strong state-of-the-art policies and controlled ablations of our own method. External baselines include ACT (Zhao et al., 2023), Diffusion Policy (Chi et al., 2025) and  $\pi_0$  (Black et al., 2024). We also include a standard “ACT + Tactile” baseline to isolate whether the performance gain comes from the complex “Dreaming” architecture or simply from the availability of tactile data. We also evaluate several variants of our model:

Ours (HSA-Only, No Dream): Stage-1 variant that uses HSA-aligned encoders but relies solely on the current state, removing the contribution of the world model.

Ours (No HSA, Dream-Only): Ablation trained without the  $\mathcal{L}_{HSA}$  loss, used to test whether spatial alignment can be learned implicitly.

Ours (HSA & Dream): Our full Stage-2 model incorporating both the HSA and the Think–Dream–Act pipeline.

## 4.2 Main Results

We evaluate all models by measuring their task success rate (SR) over 100 trials for each task in four real world tasks. As shown in Table 1, our full model achieves the highest performance across all contact-rich manipulation tasks.

Vision-only baselines (ACT (Zhao et al., 2023), Diffusion Policy (Chi et al., 2025)) perform poorly, especially on tasks like USB Insertion and Gear Assembly, where visual ambiguity and depth occlusion are significant. The Diffusion

Policy baseline demonstrates moderate competence but fails to capture the fine-grained temporal consistency required for stable contact handling, often oscillating or prematurely retracting during insertion. The ACT with tactile baseline also shows that tactile modality can bring some performance gain but to use our HSA and ‘Dream’ method can better utilize it.

DreamTacVLA consistently outperforms all baseline and ablated models, with the best performance observed in USB Insertion and Peg-in-Hole. Both tasks demand precise micro-slip perception, iterative pose refinement, and stable contact maintenance. These capabilities are difficult to achieve with vision-only or feedforward tactile policies. The Think-Dream-Act mechanism is particularly influential in these settings: as the end-effector approaches the socket or hole, the policy executes controlled residual adjustments rather than committing to a simple open-loop motion. This behavior indicates that the tactile world model provides high-frequency predictive feedback that guides fine-grained corrections.

These benefits are especially pronounced in Peg-in-Hole, a task where small variations in initial grasp or wrist orientation frequently lead to failure for baselines and ablations. DreamTacVLA handles such variations reliably, even when trained with only 50 demonstrations, suggesting that the combination of high-resolution tactile sensing, Hierarchical Spatial Alignment (HSA) and temporal tactile prediction provides strong physical grounding. The model not only predicts local contact dynamics but also leverages them for robust online refinement, resulting in higher success rates and improved generalization under perturbations.

## 4.3 Ablation Studies

We conduct detailed ablations to validate our key design choices.

**Effect of HSA and World Model.** As shown in Table 1, Although the policy still attempts continuous corrections, it frequently misaligns with the socket or hole and fails to recover, revealing that spatial grounding cannot be learned implicitly. Removing the world model (“HSA-Only”) preserves coarse alignment but removes temporal foresight; without draft refinement from the dreaming stage, the policy no longer performs the fine residual adjustments needed near the target and behaves inconsistently. The full model (HSA + World Model) achieves an average 22.3% improvement over both ablations, demonstrating that reliable insertion behavior emerges only when spatial grounding and temporal imagination are combined.

**World Model Sizes.** We ablate the components of our world model ( $\mathcal{L}_W$ ). As shown in Figure 8, training a world model to predict *only* future visual images (like DreamVLA (Zhang et al., 2025)) provides a minor boost. The tactile forecast is

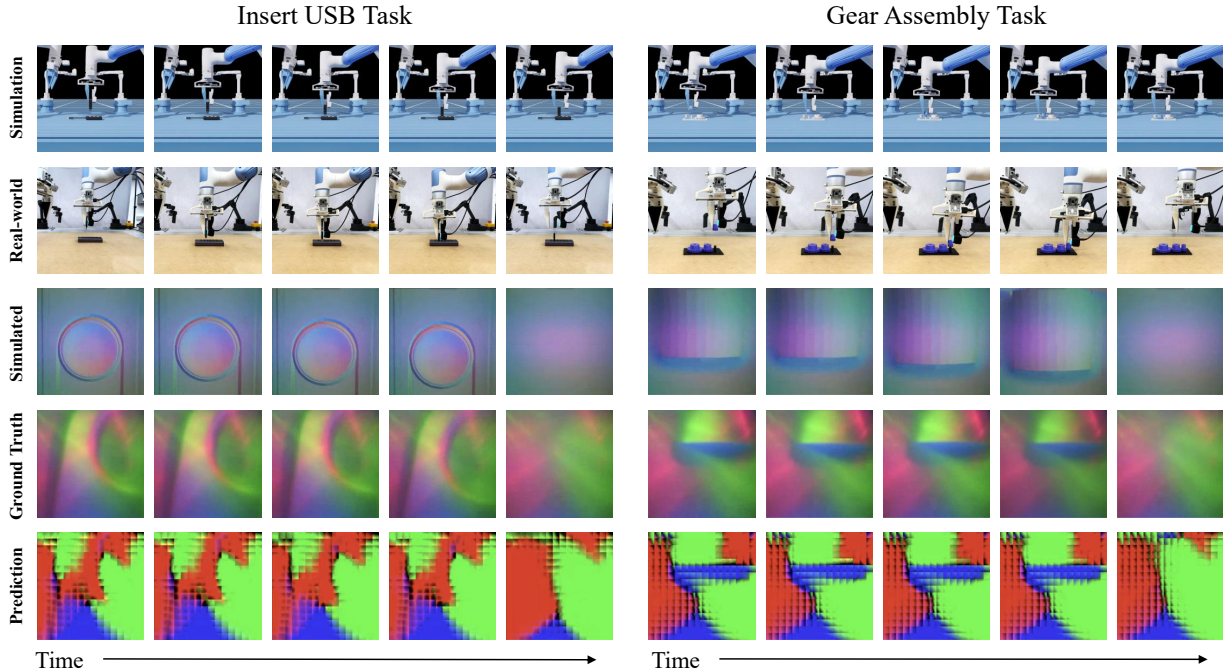


Figure 7. Qualitative comparison of our model’s tactile prediction. For both the Peginhole and Tool Stabilization tasks, we visualize the sequence (left to right) comparing our model’s Prediction (bottom row) to the Ground Truth tactile data (fourth row). The corresponding tactile images are provide as well.

the most critical component. However, training the model to predict *all* future modalities (Tactile+Vision) yields the best results, as it learns a more consistent cross-modal physics model.

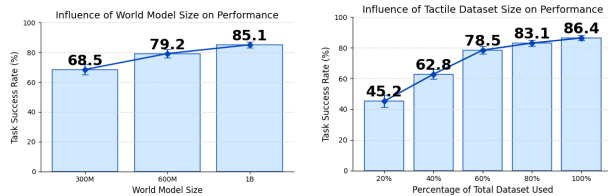


Figure 8. Ablation studies on model and data scaling.

**Tactile Dataset Size.** We further investigated the influence of the tactile dataset size on our model’s performance. To do this, we trained separate instances of our model using progressively larger subsets of our collected data, ranging from 20% to 100% of the total available samples. Figure 8 illustrates the relationship between dataset size and task success rate. We observed a consistent improvement in performance as the number of training data increased. In particular, the model begins to converge towards stable performance at approximately 60% of the dataset size, suggesting that our current data collection is sufficient for the investigated tasks. However, the continued slight upward trend indicates that further scaling of various tactile data could yield additional, albeit diminishing, marginal gains.

## 5 Conclusion

We present DreamTacVLA, a physically grounded Vision-Language-Action framework that addresses the contact-blindness of vision-centric policies. The method combines a Hierarchical Spatial Alignment (HSA) loss that tightly grounds tactile, wrist, and third-person cues, and a Think–Dream–Act strategy that uses a tactile world model to forecast visuotactile outcomes of draft actions, enabling anticipatory contact reasoning.

Across four contact-rich manipulation tasks, DreamTacVLA consistently surpasses vision-only and force-based baselines and achieves near-perfect performance in both simulation and real settings. Ablation studies confirm the complementary roles of tactile grounding and tactile forecasting.

Although Think–Dream–Act adds inference overhead, future work will explore policy distillation and adaptive dreaming for faster single-pass reasoning. Scaling tactile world models with larger multimodal corpora offers a path toward more general agents that can reason about physical interactions with human-like intuition.

## References

- Assran, M., Bardes, A., Fan, D., Garrido, Q., Howes, R., Muckley, M., Rizvi, A., Roberts, C., Sinha, K., Zholus, A., et al. V-jepa 2: Self-supervised video models enable understanding, prediction and planning. *arXiv preprint arXiv:2506.09985*, 2025.
- Bhirangi, R., Pattabiraman, V., Erciyes, E., Cao, Y., Hellebrekers, T., and Pinto, L. Anyskin: Plug-and-play skin sensing for robotic touch. In *2025 IEEE International Conference on Robotics and Automation (ICRA)*, pp. 16563–16570. IEEE, 2025.
- Bjorck, J., Castañeda, F., Cherniadev, N., Da, X., Ding, R., Fan, L., Fang, Y., Fox, D., Hu, F., Huang, S., et al. Gr00t n1: An open foundation model for generalist humanoid robots. *arXiv preprint arXiv:2503.14734*, 2025.
- Black, K., Brown, N., Driess, D., Esmail, A., Equi, M., Finn, C., Fusai, N., Groom, L., Hausman, K., Ichter, B., et al.  $\pi_0$ : A vision-language-action flow model for general robot control. *arXiv preprint arXiv:2410.24164*, 2024.
- Brohan, A., Brown, N., Carbajal, J., Chebotar, Y., Dabis, J., Finn, C., Gopalakrishnan, K., Hausman, K., Herzog, A., Hsu, J., et al. Rt-1: Robotics transformer for real-world control at scale. *arXiv preprint arXiv:2212.06817*, 2022.
- Brohan, A., Brown, N., Carbajal, J., Chebotar, Y., Chen, X., Choromanski, K., Ding, T., Driess, D., Dubey, A., Finn, C., et al. Rt-2: Vision-language-action models transfer web knowledge to robotic control, 2023. *URL <https://arxiv.org/abs/2307.15818>*, 2024.
- Cen, J., Yu, C., Yuan, H., Jiang, Y., Huang, S., Guo, J., Li, X., Song, Y., Luo, H., Wang, F., et al. Worldvla: Towards autoregressive action world model. *arXiv preprint arXiv:2506.21539*, 2025.
- Cheng, Z., Zhang, Y., Zhang, W., Li, H., Wang, K., Song, L., and Zhang, H. Omnivtla: Vision-tactile-language-action model with semantic-aligned tactile sensing. *arXiv preprint arXiv:2508.08706*, 2025.
- Chi, C., Xu, Z., Feng, S., Cousineau, E., Du, Y., Burchfiel, B., Tedrake, R., and Song, S. Diffusion policy: Visuomotor policy learning via action diffusion. *The International Journal of Robotics Research*, 44(10-11): 1684–1704, 2025.
- Fu, L., Datta, G., Huang, H., Panitch, W. C.-H., Drake, J., Ortiz, J., Mukadam, M., Lambeta, M., Calandra, R., and Goldberg, K. A touch, vision, and language dataset for multimodal alignment. *arXiv preprint arXiv:2402.13232*, 2024.
- Ha, D. and Schmidhuber, J. World models. *arXiv preprint arXiv:1803.10122*, 2(3), 2018.
- Hafner, D., Pasukonis, J., Ba, J., and Lillicrap, T. Mastering diverse domains through world models. *arXiv preprint arXiv:2301.04104*, 2023.
- He, K., Zhang, X., Ren, S., and Sun, J. Deep residual learning for image recognition. In *Proceedings of the IEEE Conference on Computer Vision and Pattern Recognition (CVPR)*, pp. 770–778, 2016.
- Heng, L., Geng, H., Zhang, K., Abbeel, P., and Malik, J. Vitacformer: Learning cross-modal representation for visuo-tactile dexterous manipulation. *arXiv preprint arXiv:2506.15953*, 2025.
- Higuera, C., Sharma, A., Bodduluri, C. K., Fan, T., Lancaster, P., Kalakrishnan, M., Kaess, M., Boots, B., Lambeta, M., Wu, T., et al. Sparsh: Self-supervised touch representations for vision-based tactile sensing. *arXiv preprint arXiv:2410.24090*, 2024.
- Huang, J., Wang, S., Lin, F., Hu, Y., Wen, C., and Gao, Y. Tactile-vla: Unlocking vision-language-action model’s physical knowledge for tactile generalization. *arXiv preprint arXiv:2507.09160*, 2025.
- Intelligence, P., Black, K., Brown, N., Darpinian, J., Dhabalia, K., Driess, D., Esmail, A., Equi, M., Finn, C., Fusai, N., et al.  $\pi_{0.5}$ : A vision-language-action model with open-world generalization. *arXiv preprint arXiv:2504.16054*, 2025.
- Jones, J., Mees, O., Sferrazza, C., Stachowicz, K., Abbeel, P., and Levine, S. Beyond sight: Finetuning generalist robot policies with heterogeneous sensors via language grounding. *arXiv preprint arXiv:2501.04693*, 2025.
- Kim, M. J., Pertsch, K., Karamcheti, S., Xiao, T., Balakrishna, A., Nair, S., Rafailov, R., Foster, E., Lam, G., Sankeki, P., et al. Openvla: An open-source vision-language-action model. *arXiv preprint arXiv:2406.09246*, 2024.
- Kim, M. J., Finn, C., and Liang, P. Fine-tuning vision-language-action models: Optimizing speed and success. *arXiv preprint arXiv:2502.19645*, 2025.
- Lambeta, M., Chou, P.-W., Tian, S., Yang, B., Maloon, B., Most, V. R., Stroud, D., Santos, R., Byagowi, A., Kammerer, G., et al. Digit: A novel design for a low-cost compact high-resolution tactile sensor with application to in-hand manipulation. *IEEE Robotics and Automation Letters*, 5(3):3838–3845, 2020.
- Li, C., Wen, J., Peng, Y., Peng, Y., Feng, F., and Zhu, Y. Pointvla: Injecting the 3d world into vision-language-action models. *arXiv preprint arXiv:2503.07511*, 2025.

- Li, H., Zhang, Y., Zhu, J., Wang, S., Lee, M. A., Xu, H., Adelson, E., Fei-Fei, L., Gao, R., and Wu, J. See, hear, and feel: Smart sensory fusion for robotic manipulation. *arXiv preprint arXiv:2212.03858*, 2022.
- Li, Q., Liang, Y., Wang, Z., Luo, L., Chen, X., Liao, M., Wei, F., Deng, Y., Xu, S., Zhang, Y., et al. Cogact: A foundational vision-language-action model for synergizing cognition and action in robotic manipulation. *arXiv preprint arXiv:2411.19650*, 2024.
- Lin, T., Li, G., Zhong, Y., Zou, Y., Du, Y., Liu, J., Gu, E., and Zhao, B. Evo-0: Vision-language-action model with implicit spatial understanding. *arXiv preprint arXiv:2507.00416*, 2025.
- Liu, S., Wu, L., Li, B., Tan, H., Chen, H., Wang, Z., Xu, K., Su, H., and Zhu, J. Rdt-1b: a diffusion foundation model for bimanual manipulation. *arXiv preprint arXiv:2410.07864*, 2024.
- Liu, Z., Liu, J., Xu, J., Han, N., Gu, C., Chen, H., Zhou, K., Zhang, R., Hsieh, K. C., Wu, K., et al. Mla: A multisensory language-action model for multimodal understanding and forecasting in robotic manipulation. *arXiv preprint arXiv:2509.26642*, 2025.
- Nair, S., Rajeswaran, A., Kumar, V., Finn, C., and Gupta, A. R3m: A universal visual representation for robot manipulation. *arXiv preprint arXiv:2203.12601*, 2022.
- Nguyen, D. H., Schneider, T., Duret, G., Kshirsagar, A., Belousov, B., and Peters, J. Tacex: Gelsight tactile simulation in isaac sim—combining soft-body and visuotactile simulators. *arXiv preprint arXiv:2411.04776*, 2024.
- NVIDIA. Isaac Sim. URL <https://github.com/isaac-sim/IsaacSim>.
- O’Neill, A., Rehman, A., Maddukuri, A., Gupta, A., Padalkar, A., Lee, A., Pooley, A., Gupta, A., Mandelkar, A., Jain, A., et al. Open x-embodiment: Robotic learning datasets and rt-x models: Open x-embodiment collaboration 0. In *2024 IEEE International Conference on Robotics and Automation (ICRA)*, pp. 6892–6903. IEEE, 2024.
- Qu, D., Song, H., Chen, Q., Yao, Y., Ye, X., Ding, Y., Wang, Z., Gu, J., Zhao, B., Wang, D., et al. Spatialvla: Exploring spatial representations for visual-language-action model. *arXiv preprint arXiv:2501.15830*, 2025.
- Radford, A., Kim, J. W., Hallacy, C., Ramesh, A., Goh, G., Agarwal, S., Sastry, G., Askell, A., Mishkin, P., Clark, J., et al. Learning transferable visual models from natural language supervision. In *International conference on machine learning*, pp. 8748–8763. PmLR, 2021.
- She, Z., Wang, S., Lee, G., and Su, H. Tactile-based policy learning for contact-rich tasks. *Robotics and Autonomous Systems*, 2023.
- Si, Z. and Yuan, W. Taxim: An example-based simulation model for gelsight tactile sensors. *IEEE Robotics and Automation Letters*, 7(2):2361–2368, 2022.
- Team, O. M., Ghosh, D., Walke, H., Pertsch, K., Black, K., Mees, O., Dasari, S., Hejna, J., Kreiman, T., Xu, C., et al. Octo: An open-source generalist robot policy. *arXiv preprint arXiv:2405.12213*, 2024.
- Wu, Z., Lin, Y., Zhao, Y., Zhang, X., Chen, Z., Lepora, N., and Luo, S. Vitacgen: Robotic pushing with vision-to-touch generation. *IEEE Robotics and Automation Letters*, 2025.
- Xue, H., Ren, J., Chen, W., Zhang, G., Fang, Y., Gu, G., Xu, H., and Lu, C. Reactive diffusion policy: Slow-fast visual-tactile policy learning for contact-rich manipulation. *arXiv preprint arXiv:2503.02881*, 2025.
- Yang, F., Feng, C., Chen, Z., Park, H., Wang, D., Dou, Y., Zeng, Z., Chen, X., Gangopadhyay, R., Owens, A., et al. Binding touch to everything: Learning unified multimodal tactile representations. In *Proceedings of the IEEE/CVF Conference on Computer Vision and Pattern Recognition*, pp. 26340–26353, 2024.
- Yuan, W., Dong, S., and Adelson, E. H. Gelsight: High-resolution tactile sensing for geometry and force. *Conference on Computer Vision and Pattern Recognition (CVPR)*, 2017.
- Zhang, W., Liu, H., Qi, Z., Wang, Y., Yu, X., Zhang, J., Dong, R., He, J., Lu, F., Wang, H., et al. Dreamvla: a vision-language-action model dreamed with comprehensive world knowledge. *arXiv preprint arXiv:2507.04447*, 2025.
- Zhao, J., Ma, Y., Wang, L., and Adelson, E. H. Transferable tactile transformers for representation learning across diverse sensors and tasks. *arXiv preprint arXiv:2406.13640*, 2024.
- Zhao, T. Z., Kumar, V., Levine, S., and Finn, C. Learning fine-grained bimanual manipulation with low-cost hardware. *arXiv preprint arXiv:2304.13705*, 2023.
- Zheng, R., Liang, Y., Huang, S., Gao, J., Daumé III, H., Kolobov, A., Huang, F., and Yang, J. Tracevla: Visual trace prompting enhances spatial-temporal awareness for generalist robotic policies. *arXiv preprint arXiv:2412.10345*, 2024.

## Appendix Catalogue

This appendix provides additional implementation details, experimental results, and theoretical background for DreamTacVLA. Below is a summary of the contents:

|  |           |
|--|-----------|
| <b>Appendix A: Simulation Pipeline and Large-Scale Data Collection</b> | <b>11</b> |
| <b>Appendix B: Implementation Details</b>                              | <b>12</b> |
| <b>Appendix C: Hierarchical Spatial Alignment (HSA)</b>                | <b>13</b> |
| <b>Appendix D: Tactile World Model Pretraining and Forecasting</b>     | <b>15</b> |
| <b>Appendix E: Evaluation Protocol</b>                                 | <b>16</b> |
| <b>Appendix F: Extended Related Work</b>                               | <b>17</b> |

## A Simulation Pipeline and Large-Scale Data Collection

This section clarifies the role of simulation in DreamTacVLA and explains data quality, expert reliability, and sim-to-real validity. Simulation is used not as a proxy for deployment, but as a scalable and stable substrate for learning spatially grounded tactile representations and tactile future prediction.

### A.1 IsaacSim Environment

All simulation experiments are conducted in NVIDIA IsaacSim with GPU-accelerated PhysX, using conservative physics settings to ensure stable long-horizon contact under tight tolerances. The simulated robot is a digital twin of the Dobot XTrainer with shared camera extrinsics between simulation and real-world setups. Following the main submission, we employ a high-fidelity visuotactile simulator based on TacEx and Taxim-style optical and marker-texture warping to synthesize GelSight-like tactile observations, enabling large-scale data collection under randomized object poses in parallel simulation environments.

Table 2. Simulation configuration (IsaacSim).

| Component             | Setting                          |
|-----------------------|----------------------------------|
| Physics timestep      | 1/60 s                           |
| Solver substeps       | 2                                |
| Control frequency     | 30 Hz                            |
| Max episode length    | 300 steps                        |
| Parallel environments | 1024 / GPU(24G)                  |
| Sensors               | TPV RGB, Wrist RGB, Dual Tactile |

### A.2 Automated Expert Demonstrations (cuRobo)

Expert demonstrations are not collected via human teleoperation. Instead, we employ an automated, privileged expert based on cuRobo, which has access to ground-truth object pose, collision geometry, and task-specific termination conditions. The expert operates in task space and generates collision-aware trajectories that satisfy geometric alignment and insertion constraints. These trajectories are time-parameterized (minimum-jerk) and resampled at the control frequency (30 Hz) to produce per-step 6D end-effector  $\Delta$ -pose + gripper supervision, consistent with the action representation used by the policy, resulting in low-noise and consistent demonstrations for contact-rich manipulation.

Table 3. cuRobo expert trajectory generation.

| Aspect             | Specification               |
|--------------------|-----------------------------|
| Planner            | cuRobo (batched)            |
| Batch size         | 256 queries                 |
| Planning horizon   | 32 waypoints (minimum-jerk) |
| Collision checking | Robot + objects + table     |
| IK tolerance       | 2 mm position / 2° rotation |
| Action format      | 6D EE delta pose + gripper  |

This design guarantees demonstration quality: stable contact behavior at sub-millimeter precision would be extremely difficult to achieve via human teleoperation without force or tactile feedback.

Table 4. Task success rate (%) in IsaacSim (100 trials per task).

| Model                         | Peg-in-Hole | USB Insert  | Gear Assembly | Tool Stabilization |
|-------------------------------|-------------|-------------|---------------|--------------------|
| ACT                           | 72.4        | 78.1        | 65.3          | 61.7               |
| Diffusion Policy              | 75.6        | 80.2        | 69.4          | 66.1               |
| $\pi_0$                       | 83.5        | 85.9        | 77.2          | 74.6               |
| Ours (HSA-Only, No Dream)     | 89.1        | 90.4        | 84.6          | 82.7               |
| Ours (No HSA, Dream-Only)     | 93.8        | 94.6        | 88.9          | 90.1               |
| <b>Ours (HSA &amp; Dream)</b> | <b>98.6</b> | <b>97.9</b> | <b>95.2</b>   | <b>94.7</b>        |

### A.3 Success-Based Filtering and Synchronization

Only successful rollouts are retained as demonstrations, based on task-specific geometric and temporal criteria (e.g., insertion depth, alignment error, sustained stability). All modalities are logged with strict step-level synchronization; if any modality is missing at a timestep, the entire episode is discarded. This filtering is applied only for constructing expert supervision for behavior cloning; evaluation is performed on fresh randomized initializations.

### A.4 Performance within IsaacSim

To assess the effectiveness of our method under controlled conditions, we report task success rates measured inside IsaacSim using the same evaluation protocol as in real-world experiments as Table 4 shows. These simulation-side results provide additional context that the relative performance trends and ablation ordering observed on real hardware are already consistent in IsaacSim. This consistency suggests that the benefits of HSA and Dreaming are not solely driven by real-world noise or dataset imbalance.

## B Implementation Details

### B.1 Model Architecture

**Overview.** Dream-Tac VLA uses a hybrid vision-language-action architecture that combines Action Chunking with Transformers (ACT) (Zhao et al., 2023) as the policy backbone with V-JEPA2 (Assran et al., 2025) vision encoders for tactile perception. The architecture processes multi-modal sensory inputs including RGB images from workspace cameras and tactile images from vision-based tactile sensors mounted on the gripper.

**Visual Encoders.** For RGB camera inputs, we use frozen ResNet-18 (He et al., 2016) backbones. Each RGB camera (top view and wrist cameras) has a dedicated ResNet-18 encoder. The backbone outputs are projected to the transformer hidden dimension via a  $1 \times 1$  convolution layer.

For tactile image inputs, we leverage a frozen V-JEPA2 ViT-Large (Assran et al., 2025) encoder with 1024-dimensional embeddings. The V-JEPA2 encoder is pretrained on large-scale video data and produces rich spatiotemporal representations. To adapt these frozen representations to our downstream manipulation tasks while preserving the pretrained knowledge, we introduce learnable residual adapters on top of the ViT encoder.

**Residual Adapter Architecture.** The residual adapter operates on patch-level tokens from the frozen ViT encoder. Given patch tokens  $\mathbf{z} \in \mathbb{R}^{N \times D}$  where  $N$  is the number of patches and  $D = 1024$  is the embedding dimension, the adapter applies:

$$\mathbf{z}' = \mathbf{z} + \alpha \cdot \text{MLP}(\text{LayerNorm}(\mathbf{z})) \quad (\text{B.1})$$

where  $\alpha$  is a learnable scaling parameter initialized to 0.1 for training stability. The MLP consists of 3 layers with hidden dimension 512, GELU activations, and dropout rate 0.1. The adapted patch tokens are then aggregated using attention pooling with a learnable query token:

$$\mathbf{h}_\tau = \text{AttentionPool}(\mathbf{z}') \in \mathbb{R}^D \quad (\text{B.2})$$

This architecture enables task-specific adaptation of the frozen V-JEPA2 representations with only  $\sim 1.5\text{M}$  additional trainable parameters per tactile encoder.

**Transformer Architecture.** The policy transformer follows the ACT architecture with a CVAE-style encoder-decoder structure:

- **CVAE Encoder:** 4-layer transformer encoder with hidden dimension 512, 8 attention heads, feed-forward dimension 3200, and dropout 0.1. The encoder produces a 32-dimensional latent code during training.
- **Action Decoder:** 7-layer transformer decoder with the same hidden dimensions. The decoder takes as input learnable action queries, proprioceptive state embedding, and the latent code.
- **Action Chunk Size:** 45 timesteps, enabling temporal action prediction for smooth execution.

**Fusion Strategy.** Visual features from all cameras (RGB and tactile) are concatenated along the sequence dimension before being processed by the transformer decoder. Specifically, ResNet features are flattened to  $H \times W$  tokens per RGB camera, and tactile features contribute 1 pooled token per sensor. Sinusoidal positional embeddings are used for RGB features, and learnable position embeddings are used for tactile and proprioceptive tokens.

## B.2 Training Details

We use AdamW (He et al., 2016) optimizer with the following hyperparameters as shown in Table 5. For RGB images, we apply color jitter augmentation with brightness=0.3, contrast=0.4, saturation=0.5, and hue=0.08 when using diffusion-based policies. Tactile images are only resized to  $224 \times 224$  without additional augmentation to preserve contact pattern fidelity. Actions and proprioceptive states are normalized using per-dimension mean and standard deviation computed from the training set. Images are normalized using ImageNet statistics (mean=[0.485, 0.456, 0.406], std=[0.229, 0.224, 0.225]). Training is performed on a single NVIDIA GPU. A typical training run of 20,000 steps takes approximately 8–12 hours depending on GPU type and dataset size. We formalize the full DreamTacVLA training sequence in Algorithm 1.

## B.3 Inference

During inference, the CVAE encoder is bypassed and the latent code is set to zero (mean of the prior). Actions are predicted in chunks of 45 timesteps. We use temporal aggregation with exponential weighting to smooth action execution:

$$a_t = \sum_{k=0}^K w_k \cdot a_t^{(k)} \quad (\text{B.3})$$

where  $a_t^{(k)}$  is the action at time  $t$  predicted  $k$  steps ago, and  $w_k \propto \exp(-\lambda k)$  are exponentially decaying weights. The control loop runs at 50 Hz to match the data collection frequency.

# C Hierarchical Spatial Alignment (HSA)

## C.1 Sensor and Camera Calibration

**Extrinsics.** We calibrate the rigid transforms from robot base to each camera frame (third-person and wrist) using a standard hand–eye calibration procedure. Let  $T_c^b$  denote camera extrinsics in the base frame, and  $T_{ee}^b$  the end-effector pose from forward kinematics computed using Denavit-Hartenberg (DH) parameters for the Nova 2 robot as shown in Table 6. The tactile sensor pose  $T_{\text{sensor}}^b(t)$  is obtained via a fixed transform  $T_{\text{sensor}}^{ee}$  mounted on the gripper:  $T_{\text{sensor}}^b(t) = T_{ee}^b T_{\text{sensor}}^{ee}$ , where

$$T_c^b = \begin{bmatrix} 1.0 & 0.0 & 0.0 & 0.7 \\ 0.0 & -1.0 & 0.0 & -0.49 \\ 0.0 & 0.0 & 1.0 & 1.14 \\ 0.0 & 0.0 & 0.0 & 1.0 \end{bmatrix}$$

**Intrinsics.** For each camera, we use intrinsic matrix  $K$  and distortion coefficients from calibration. If images are undistorted online, the projection below assumes the rectified pinhole model. In our case, the value of  $K$  is

$$K = \begin{bmatrix} 647.0 & 0.0 & 653.0 \\ 0.0 & 644.0 & 364.0 \\ 0.0 & 0.0 & 1.0 \end{bmatrix}$$

| Hyperparameter                      | Value                  |
|-------------------------------------|------------------------|
| <i>Transformer</i>                  |                        |
| Hidden dimension                    | 512                    |
| Feed-forward dimension              | 3200                   |
| Encoder layers                      | 4                      |
| Decoder layers                      | 7                      |
| Attention heads                     | 8                      |
| Dropout                             | 0.1                    |
| Latent dimension (CVAE)             | 32                     |
| Action chunk size                   | 45                     |
| <i>Visual Encoders</i>              |                        |
| RGB backbone                        | ResNet-18 (frozen)     |
| RGB input resolution                | 640 × 480              |
| Tactile encoder                     | V-JEPA2 ViT-L (frozen) |
| Tactile embedding dim               | 1024                   |
| Tactile input resolution            | 224 × 224              |
| <i>Residual Adapter</i>             |                        |
| Hidden dimension                    | 512                    |
| Depth (layers)                      | 3                      |
| Dropout                             | 0.1                    |
| Scale init ( $\alpha$ )             | 0.1                    |
| Pooling                             | Attention              |
| <i>HSA Loss</i>                     |                        |
| Temperature ( $\kappa$ )            | 0.07                   |
| Feature extractor                   | ViT-B/16               |
| HSA weight ( $\beta_{\text{HSA}}$ ) | 1.0                    |
| <i>Training</i>                     |                        |
| Optimizer                           | AdamW                  |
| Learning rate                       | $1 \times 10^{-5}$     |
| Backbone learning rate              | $1 \times 10^{-5}$     |
| Weight decay                        | $1 \times 10^{-4}$     |
| Batch size                          | 16                     |
| KL weight ( $\beta_{\text{KL}}$ )   | 10                     |
| Training steps                      | 10,000–20,000          |

Table 5. Complete hyperparameter configuration for Dream-Tac VLA.

## C.2 Projecting Tactile Sensor to Image Bounding Boxes

To localize the tactile sensor in the wrist and third-person images for HSA, we project a set of 3D points that approximate the tactile sensor’s visible surface (e.g., 4 corners of a small rectangle / circle sample points) from the sensor frame into each camera:  $\mathbf{u} \sim K {}^cT_b \mathbf{X}_b$ ,  $\mathbf{X}_b = {}^bT_{\text{sensor}}(t) \mathbf{X}_{\text{sensor}}$ . We then take the min/max pixel coordinates over the projected points to form bounding boxes  $B_w^{(t)}$  and  $B_{tp}^{(t)}$ . We clip boxes to image bounds and discard frames where (i) the box is fully out of view or (ii) projected depth is negative. We optionally enlarge the boxes by a small margin (e.g., 5–15 pixels) to tolerate calibration noise. If the tactile sensor is occluded in third-person view (common), we keep  $B_{tp}$  but down-weight the TPV term in  $L_{\text{HSA}}$  (see Sec. 9.4) or mask it when visibility checks fail.

## C.3 Mapping Bounding Boxes to Patch Tokens

For CLIP ViT-L/14 inputs of resolution  $224 \times 224$  and patch size 16, the patch grid is  $16 \times 16$ . We map bounding box pixels  $[x_0, x_1] \times [y_0, y_1]$  to patch indices:

$$i \in \left[ \left\lfloor \frac{x_0}{14} \right\rfloor, \left\lfloor \frac{x_1}{14} \right\rfloor \right], \quad j \in \left[ \left\lfloor \frac{y_0}{14} \right\rfloor, \left\lfloor \frac{y_1}{14} \right\rfloor \right].$$

Tokens whose patch centers fall inside the box are selected and mean-pooled to form  $h_w$  and  $h_{tp}$ . The tactile embedding  $h_\tau$  is mean-pooled from tactile tokens (or from the pooled tactile representation if a pooling head is used).

| Joint | $\theta$      | $d$ (m) | $a$ (m) | $\alpha$ |
|-------|---------------|---------|---------|----------|
| 1     | $q_0$         | 0.2234  | 0       | $\pi/2$  |
| 2     | $q_1 - \pi/2$ | 0       | -0.280  | 0        |
| 3     | $q_2$         | 0       | -0.225  | 0        |
| 4     | $q_3 - \pi/2$ | 0.1175  | 0       | $\pi/2$  |
| 5     | $q_4$         | 0.120   | 0       | $-\pi/2$ |
| 6     | $q_5$         | 0.088   | 0       | 0        |

Table 6. DH parameters for Dobot Nova 2 robot.

#### C.4 HSA Loss: Negatives, Temperature, and Weighting

We compute InfoNCE losses for tactile–wrist and tactile–TPV alignment:

$$L_{HSA} = L_{HSA-W} + L_{HSA-TP}.$$

**Negatives.** We use a mix of: in-image negatives: patches outside the bounding box (hard negatives), in-batch negatives: patches from other samples in the batch (diverse negatives).

**Temperature.** We set  $\kappa$  to a fixed value (0.07) and keep it constant across training.

**Visibility-aware weighting.** If TPV visibility is unreliable, we apply  $L_{HSA} = L_{HSA-W} + \alpha(t) L_{HSA-TP}$ , where  $\alpha(t) \in [0, 1]$  is set based on projection validity / confidence.

## D Tactile World Model Pretraining and Forecasting Loss

To train our tactile world model, we adopt a self-supervised latent-prediction approach inspired by the **V-JEPA** (Video Joint-Embedding Predictive Architecture) framework. This approach shifts the learning objective from raw sensor reconstruction to the prediction of abstract latent representations.

### D.1 Latent Masked Forecasting via Teacher Forcing

The pretraining phase utilizes a *teacher-student* architecture to facilitate stable feature extraction from tactile sequences. This process is defined by two primary components:

- **Teacher Encoder:** The teacher receives the complete, unmasked tactile sequence and generates target embeddings. To maintain a stable training target and prevent representation collapse, the teacher’s weights are updated using an Exponential Moving Average (EMA) of the student’s parameters rather than through direct backpropagation.
- **Student Predictor:** The student is provided with a temporally masked spatial version of the tactile sequence. Its objective is to predict the latent representations of the missing patches, conditioned on the available context and the specific positional encodings of the masked regions.

### D.2 Forecasting Loss Function

The world model is optimized by minimizing the  $L_2$  distance between the student’s predicted embeddings and the teacher’s ground-truth embeddings in the latent space. Critically, the loss is calculated only over the masked indices  $M$ .

The forecasting loss  $\mathcal{L}$  is formulated as:

$$\mathcal{L} = \sum_{t \in M} \|z_{teacher}(t) - \hat{z}_{student}(t)\|_2^2 \quad (\text{D.1})$$

where  $z_{teacher}(t)$  represents the latent target produced by the EMA-updated teacher, and  $\hat{z}_{student}(t)$  represents the student’s prediction for the corresponding masked segment. By training in this latent space, the model learns to capture the underlying physics of tactile interaction—such as shear forces and surface geometry—while remaining robust to the inherent sensor noise found in raw tactile data.

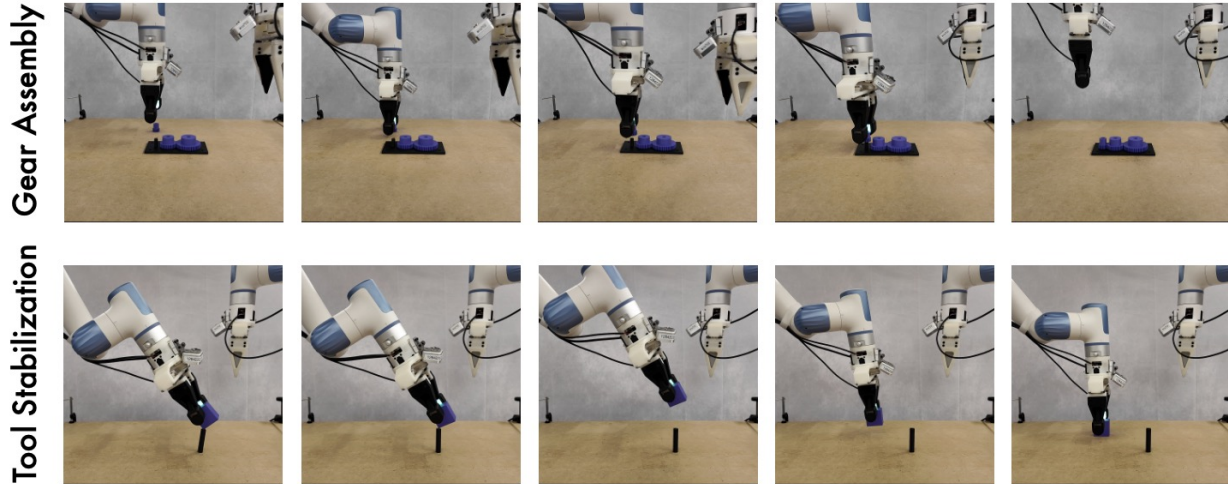


Figure 9. Keyframes of the gear assembly and tool stabilization task workflow.



Figure 10. Keyframes of one example failure case.

### D.3 Pretraining Data and Temporal Sampling

We pretrain the tactile world model on unlabeled tactile sequences extracted from both simulation and real demonstrations. We sample short clips of length  $T$  with stride  $s$ , and randomly choose a prediction horizon  $N \in \{1, \dots, N_{\max}\}$ . This yields pairs  $(I_{\tau}^{(t)}, I_{\tau}^{(t+N)})$  to encourage multi-step predictive structure.

## E Evaluation

To evaluate the efficacy of our framework, we conducted extensive experiments on a dual-arm manipulation platform. Our evaluation focuses on the system’s ability to perform high-precision tasks where visual and tactile integration is critical.

The hardware setup consists of a Dobot X-Trainer dual-arm system. The sensing suite are two wrist-mounted cameras provide localized views of the grippers, while a single overhead camera captures the global workspace and a GelSight Digit sensor is integrated into the end-effector, providing high-resolution tactile feedback of the contact geometry.

During evaluation, objects are placed at fixed initial positions. This protocol allows us to isolate and measure the model’s performance on *precision-based* execution and fine-grained adjustments, effectively decoupling the control performance from variables associated with open-world localization. To ensure the statistical significance of our results and assess the reliability of the framework, we conducted over 100 trials for each task. This extensive testing allows us to accurately characterize the success rate and error distributions of the system. We show the rollout sequences of gear assembly and tool stabilization task at Figure 9. A failure case for Peg In Hole task is also shown at Figure 10. All the videos and source code can be found at supplementary materials.

## F Extended Related Work

### F.1 Vision-Language-Action (VLA) Models

Vision-Language-Action (VLA) models unify perception, language understanding, and action generation into a single policy for general-purpose robot control. Large-scale systems such as RT-1 (Brohan et al., 2022) and RT-2 (Brohan et al., 2024) demonstrate that scaling data and model capacity enables strong cross-task and cross-embodiment generalization. Subsequent work extends this paradigm across embodiments, datasets, and action spaces, including Open X-Embodiment (O’Neill et al., 2024), OpenVLA (Kim et al., 2024), Octo (Team et al., 2024), RDT-1B (Liu et al., 2024),  $\pi_0$  (Black et al., 2024),  $\pi_{0.5}$  (Intelligence et al., 2025), and GR00T N1 (Bjorck et al., 2025).

Beyond scale, architectural and training refinements further improve VLA effectiveness, including diffusion-based action generation (Chi et al., 2025) and language-conditioned visuomotor learning for compositional generalization (Zhao et al., 2023). Modular designs such as CogACT (Li et al., 2024) decouple high-level reasoning from low-level control, and optimized adaptation strategies like OpenVLA-OFT (Kim et al., 2025) show that carefully designed fine-tuning can significantly boost real-robot performance and efficiency.

Despite these advances, most VLA models remain vision-centric and struggle in contact-rich manipulation, where RGB observations alone cannot resolve contact state, friction, or incipient slip. Recent work such as FuSe (Jones et al., 2025) explores post-hoc adaptation with tactile and audio signals, but tactile is often treated as auxiliary rather than being integrated into perception, prediction, and action generation.

### F.2 Spatial Grounding for Robotics

Spatial grounding improves visuomotor reasoning by incorporating geometric structure beyond RGB observations. Recent VLA variants introduce explicit 3D priors, including egocentric position encodings in SpatialVLA (Qu et al., 2025) and point cloud grounding in PointVLA (Li et al., 2025), which improve generalization in geometry-sensitive manipulation. Complementary approaches model spatial structure implicitly: TraceVLA (Zheng et al., 2024) encodes spatiotemporal interaction traces, while Evo-0 (Lin et al., 2025) injects implicit 3D structure into the visual backbone via architectural and training biases. These methods primarily reason at the level of object pose and scene layout, leaving contact-level geometry unmodeled.

### F.3 Tactile Grounding for Manipulation

Tactile grounding provides contact information unavailable to vision, including contact geometry, friction, and slip, which is critical for contact-rich manipulation. Early approaches rely on low-dimensional force/torque sensing, which supports contact detection and impedance control but discards spatial structure, leading to ambiguous contact states.

Beyond force-based sensing, several works integrate tactile signals into learned policies. See, Hear, and Feel (Li et al., 2022) studies structured multimodal fusion, while more recent VLA-style approaches incorporate tactile inputs directly. MLA (Liu et al., 2025), Tactile-VLA (Huang et al., 2025), OmniVTLA (Cheng et al., 2025), and RDP (Xue et al., 2025) demonstrate improved robustness via vision–tactile fusion and reactive tactile feedback, but typically operate on temporally sparse or spatially compressed tactile representations.

In parallel, tactile representation learning focuses on transferable visuotactile embeddings decoupled from control, including Binding Touch (Yang et al., 2024), TVL (Fu et al., 2024), Sparsh (Higuera et al., 2024), AnySkin (Bhirangi et al., 2025), and T3 (Zhao et al., 2024). To enrich contact signals, ViTacGen (Wu et al., 2025) synthesizes visuotactile images from RGB inputs, but remains constrained by visual observability.

In contrast, vision-based tactile sensors such as GelSight (Yuan et al., 2017) and DIGIT (Lambeta et al., 2020) provide dense micro-vision measurements of surface deformation, encoding texture, geometry, and shear-induced slip, which are essential for modeling fine-grained contact dynamics (She et al., 2023). However, existing approaches largely treat tactile sensing as an auxiliary input or a standalone representation, without tightly integrating tactile prediction into sequential decision making.

### F.4 Predictive World Models in Robotics

Predictive world models learn latent dynamics that enable anticipation of future observations for planning and control. Early work such as World Models (Ha & Schmidhuber, 2018) and Dreamer (Hafner et al., 2023) demonstrate imagination-based control via recurrent latent dynamics. Recent large-scale pretraining methods, including R3M (Nair et al., 2022)

and V-JEPA-style approaches (Assran et al., 2025), learn structured predictive representations that transfer effectively to downstream robotic tasks.

Several VLA architectures integrate predictive modeling directly into policy learning by conditioning actions on latent roll-outs, including DreamVLA (Zhang et al., 2025) and WorldVLA (Cen et al., 2025). In the tactile domain, ViTacFormer (Heng et al., 2025) explores autoregressive visuotactile prediction, but remains focused on representation learning rather than action-conditioned rollout.

Overall, existing world-model approaches predominantly operate on visual observations or abstract latents, and lack explicit mechanisms for predicting fine-grained contact evolution, motivating extensions toward tactile-aware predictive modeling.

---

**Algorithm 1** DreamTacVLA: Two-Stage Training with Think–Dream–Act (Implementation-Matched)
 

---

**Require:** Datasets:  $\mathcal{D}_1 = \{(L, s^{(t)}, I_w^{(t)}, I_{tp}^{(t)}, I_\tau^{(t)}, a_t, B^{(t)})\}$ ,  $\mathcal{D}_2 = \{(L, s^{(t)}, I_w^{(t)}, I_{tp}^{(t)}, I_\tau^{(t)}, a_t, I_\tau^{(t+N)}, B^{(t)})\}$

1:

**Require:** Modules: multimodal encoders  $E_\psi$ , policy  $\pi_\theta$ , tactile world encoder  $W_\phi$  (pretrained, frozen), forecasting MLP  $F_\eta$

2:

**Require:** Hyperparams:  $S_1, S_2, \lambda_{HSA}, \lambda_W, \lambda_{action}$ ; null-dream token  $H_{\text{null}}$  (zeros or learned)

3: Initialize  $E_\psi, \pi_\theta$

4: Set  $H_{\text{null}}$

5: **// Stage 1: Pre-train encoders + policy with Action + HSA (no dreaming)**

6: **for**  $s \leftarrow 1$  to  $S_1$  **do**

7:   Sample  $(L, s^{(t)}, I_w^{(t)}, I_{tp}^{(t)}, I_\tau^{(t)}, a_t, B^{(t)}) \sim \mathcal{D}_1$

8:    $H_{\text{align}}^{(t)} \leftarrow E_\psi(L, I_w^{(t)}, I_{tp}^{(t)}, I_\tau^{(t)}, s^{(t)})$

9:    $L_{HSA} \leftarrow \text{HSAINFONCE}(H_{\text{align}}^{(t)}, B^{(t)})$

10:    $\hat{a}_t \leftarrow \pi_\theta(H_{\text{align}}^{(t)}, H_{\text{null}})$

11:    $L_{\text{action}} \leftarrow \text{LDIFFUSION}(\hat{a}_t, a_t)$

12:    $L \leftarrow L_{\text{action}} + \lambda_{HSA} L_{HSA}$

13:   Backprop  $L$  and update  $\psi, \theta$

14: **end for**

15: **// Stage 2: Finetune with latent dreaming (Think–Dream–Act)**

16: Load pretrained  $W_\phi$  and **freeze** it (no grad)

17: Initialize  $F_\eta$  (trainable)

18: **for**  $s \leftarrow 1$  to  $S_2$  **do**

19:   Sample  $(L, s^{(t)}, I_w^{(t)}, I_{tp}^{(t)}, I_\tau^{(t)}, a_t, I_\tau^{(t+N)}, B^{(t)}) \sim \mathcal{D}_2$

20:    $H_{\text{align}}^{(t)} \leftarrow E_\psi(L, I_w^{(t)}, I_{tp}^{(t)}, I_\tau^{(t)}, s^{(t)})$

21:    $L_{HSA} \leftarrow \text{HSAINFONCE}(H_{\text{align}}^{(t)}, B^{(t)})$

22:   **THINK:**  $a_{\text{draft}}^{(t)} \leftarrow \text{STOPGRAD}(\pi_\theta(H_{\text{align}}^{(t)}, H_{\text{null}}))$

23:   **DREAM:**  $z_\tau^{(t)} \leftarrow W_\phi(I_\tau^{(t)})$  // frozen encoder

24:    $\tilde{z}_\tau^{(t+N)} \leftarrow F_\eta(z_\tau^{(t)}, a_{\text{draft}}^{(t)})$  // predicted future latent

25:    $z_\tau^{(t+N)} \leftarrow \text{STOPGRAD}(W_\phi(I_\tau^{(t+N)}))$

26:    $L_W \leftarrow \|\tilde{z}_\tau^{(t+N)} - z_\tau^{(t+N)}\|_2^2$  // latent forecasting loss

27:   **ACT:**  $a_{\text{final}}^{(t)} \leftarrow \pi_\theta(H_{\text{align}}^{(t)}, \tilde{z}_\tau^{(t+N)})$

28:    $L_{\text{action}} \leftarrow \text{LDIFFUSION}(a_{\text{final}}^{(t)}, a_t)$

29:    $L \leftarrow \lambda_{\text{action}} L_{\text{action}} + \lambda_{HSA} L_{HSA} + \lambda_W L_W$

30:   Backprop  $L$  and update  $\psi, \theta, \eta$  //  $\phi$  stays frozen; no grad through  $a_{\text{draft}}$

31: **end for**

---